

# Critical Collapse of a Complex Scalar Field with Angular Momentum

Matthew W. Choptuik,<sup>1</sup> Eric W. Hirschmann,<sup>2</sup> Steven L. Liebling,<sup>3</sup> and Frans Pretorius<sup>4</sup>

<sup>1</sup>*CIAR Cosmology and Gravity Program*

*Department of Physics and Astronomy, University of British Columbia, Vancouver BC, V6T 1Z1 Canada*

<sup>2</sup>*Department of Physics and Astronomy, Brigham Young University, Provo, UT 84604*

<sup>3</sup>*Southampton College, Long Island University, Southampton, NY 11968*

<sup>4</sup>*Theoretical Astrophysics, California Institute of Technology, Pasadena, CA 91125*

We report a new critical solution found at the threshold of axisymmetric gravitational collapse of a complex scalar field with angular momentum. To carry angular momentum the scalar field cannot be axisymmetric; however, its azimuthal dependence is defined so that the resulting stress energy tensor and spacetime metric *are* axisymmetric. The critical solution found is non-spherical, discretely self-similar with an echoing exponent  $\Delta = 0.42 \pm 4\%$ , and exhibits a scaling exponent  $\gamma = 0.11 \pm 10\%$  in near critical collapse. Our simulations suggest that the solution is universal (within the imposed symmetry class), modulo a family-dependent constant phase in the complex plane.

The main purpose of this work is to study the effect of angular momentum in axisymmetric critical collapse of massless scalar fields. Critical collapse refers to the *threshold* of black hole formation, where interesting effects known as critical phenomena [1] have been observed in the gravitational collapse of a wide variety of types of matter, as well as vacuum gravitational waves (see [2] for recent reviews). For spherically symmetric massless scalar collapse, this behavior includes universality, scale invariance, and power law scaling of length scales that arise near criticality. In super-critical collapse, the characteristic length is the mass,  $M$ , of black holes that form. In the case of rotating collapse, since angular momentum has dimension *length*<sup>2</sup>, one might naively expect the angular momentum,  $J$ , of the black holes formed to scale as  $J \propto M^2$ . A more refined analysis carried out using perturbation theory [3] suggests that  $J \propto M^{2(1-\text{Re}[\lambda'])}$ , where  $\text{Re}[\lambda']$  is the real part of the exponent  $\lambda'$  of the dominant perturbative mode that carries angular momentum. In [4],  $\text{Re}[\lambda']$  was found to be roughly  $-0.017$ , implying an approximate scaling  $J \propto M^{2.03}$ . Thus, the Kerr parameter  $a = J/M^2$  is expected to scale to zero (albeit slowly) as the black hole threshold is approached. Incidentally, this picture could be altered significantly if the numerical evidence of [5] proves correct, and there is a *non-spherical* unstable mode of the critical solution.

In general, numerical exploration of angular momentum in the collapse of a single real scalar field would require a 3D code, for axisymmetric distributions of such a matter source cannot carry angular momentum. Constructing a general relativistic 3D simulation capable of resolving the range of length scales that unfold in scalar field critical collapse is a daunting project, and may require computational capacity not currently available. A “cheaper” alternative is to consider a set of distinct scalar fields, each with azimuthal dependence and hence angular momentum, and then add the different fields coherently such that the net stress energy tensor is axisymmetric. A natural way to achieve such a coherent sum is via a single complex field, as will be explained in

Sec. I (see [6] for an alternative approach). One drawback to this method is that imposing such an ansatz for the complex field forces a non-spherical energy distribution. This means that the class of solutions we can study occupy a region of phase space distinct from that of spherical spacetimes, and so we cannot explore the role of angular momentum as a perturbation in spherical critical collapse [1, 7]. On a positive note, the fact that we *do* find a new (axisymmetric) critical solution is interesting aside from questions of angular momentum, because it suggests that phase space has a more intricate structure than one might have naively imagined, probably containing an infinite set of distinct intermediate attractors characterized by their behavior near the center of symmetry (the results of [6] are also in accord with this conjecture). Regarding the question of how net angular momentum affects threshold behavior in this model—it appears to be irrelevant, with the angular momentum of black holes formed in super-critical collapse decaying significantly faster than  $J \propto M^2$ , though our simulations are not accurate enough to calculate exactly how fast. Below we briefly describe the physical system and numerical code we use (for more details see [5, 8, 9, 10]), and present our results in Sec. II.

## I. PHYSICAL SYSTEM

We consider the Einstein field equations

$$R_{\mu\nu} - \frac{1}{2}Rg_{\mu\nu} = 8\pi T_{\mu\nu}, \quad (1)$$

where  $g_{\mu\nu}$  is the spacetime metric,  $R_{\mu\nu}$  is the Ricci tensor,  $R \equiv R^\mu{}_\mu$  is the Ricci scalar, and we use geometric units with Newton’s constant  $G$  and the speed of light  $c$  set to 1. We use a massless, minimally-coupled, complex scalar field  $\Psi$  (with complex conjugate  $\bar{\Psi}$ ) as the matter source.  $\Psi$  satisfies a wave equation  $\Psi_{;\mu}{}^\mu = 0$ , and has a stress energy tensor  $T_{\mu\nu}$  given by

$$T_{\mu\nu} = \Psi_{;\mu}\bar{\Psi}_{;\nu} + \bar{\Psi}_{;\mu}\Psi_{;\nu} - g_{\mu\nu}\Psi_{;\gamma}\bar{\Psi}^{;\gamma}. \quad (2)$$

We solve (1) and the wave equation (hereafter the field equations) in axisymmetry, using coordinates  $[t, \rho, z, \phi]$ , where  $\phi$  is adapted to the azimuthal symmetry,  $t$  is time-like, and  $(\rho, z)$  reduce to standard cylindrical coordinates in the flatspace limit. The axial Killing vector is then

$$\xi^\nu = \left( \frac{\partial}{\partial \phi} \right)^\nu. \quad (3)$$

The existence of this Killing vector allows us to define the conserved angular momentum,  $J$ , of the spacetime

$$J = - \int_{\Sigma} T_{\mu\nu} \xi^\mu n^\nu \sqrt{h} d^3x, \quad (4)$$

where the integration is over the  $t = \text{const.}$  spacelike hypersurface,  $\Sigma$ ,  $h$  is the determinant of the intrinsic metric on  $\Sigma$ , and  $n^\mu$  is the hypersurface normal vector. Using (2) and (3), (4) evaluates to

$$J = - \int_{\Sigma} [\Psi_{,\phi} \bar{\Psi}_{;\nu} + \bar{\Psi}_{,\phi} \Psi_{;\nu}] n^\nu \sqrt{h} d^3x. \quad (5)$$

Thus, for a configuration of the scalar field to have non-zero angular momentum,  $\Psi$  must have some azimuthal dependence. We thus adopt the following ansatz

$$\Psi(\rho, z, t, \phi) \equiv \Phi(\rho, z, t) e^{im\phi} \quad (6)$$

where  $\Phi(\rho, z, t)$  is complex, and  $m$  must be an integer for the scalar field to be regular. It is straightforward to check that this form of  $\Psi$  gives a stress-energy tensor that is  $\phi$ -independent, yet can yield net angular momentum. Note that the on-axis ( $\rho = 0$ ) regularity condition for  $\Phi$  depends upon the value of  $m$ ; specifically we must have  $\lim_{\rho \rightarrow 0} \Phi(\rho, z, t) = \rho^m f(z, t)$ . For simplicity and specificity, we hereafter restrict attention to the case  $m = 1$ . As stated above, we expect that additional, distinct critical solutions exist for  $m = 2, 3, \dots$ .

To keep our discussion concise, we only state the metric and set of variables we use (all functions of  $(\rho, z, t)$ ), and briefly describe the solution procedure—more details can be found in [5, 8, 9, 10]. The line element is

$$ds^2 = -\alpha^2 dt^2 + \psi^4 [(d\rho + \beta^\rho dt)^2 + (dz + \beta^z dt)^2 + \rho^2 e^{2\rho\bar{\sigma}} d\phi^2] + (\xi_\rho d\rho + \xi_z dz) \left( 2d\phi + \frac{\xi_\rho d\rho + \xi_z dz}{\psi^4 e^{2\rho\bar{\sigma}} \rho^2} \right). \quad (7)$$

The lapse function,  $\alpha$ , is fixed by maximal slicing, and (7) reflects the additional coordinate conditions we have imposed: conformal flatness of the two dimensional  $\rho - z$  subspace, and  $\xi_t = 0$ . The Einstein equations are written in first-order-in-time form by introducing the following “conjugate” variables

$$\bar{\Omega} \equiv (-2K_\rho{}^\rho - K_z{}^z)/\rho, \quad \omega_\alpha \equiv \epsilon_{\alpha\beta\gamma\delta} \xi^\beta \xi^{\delta;\gamma}, \quad (8)$$

where  $K_\alpha{}^\beta$  is the extrinsic curvature tensor and  $\omega_\alpha$  is

the “twist” of the Killing vector. We separately evolve the real and imaginary components of the scalar field by defining real functions  $\Phi_r$  and  $\Phi_i$  via

$$\Phi \equiv \rho(\Phi_r + i\Phi_i) \quad (9)$$

and their dynamical conjugates  $\Pi_r$  and  $\Pi_i$  by

$$\Pi_r \equiv \text{Re}[\Phi_{,\alpha} n^\alpha]/\rho, \quad \Pi_i \equiv \text{Im}[\Phi_{,\alpha} n^\alpha]/\rho. \quad (10)$$

The factors of  $\rho$  appearing in the above definitions are included so that  $\Phi_r$ ,  $\Phi_i$ ,  $\Pi_r$  and  $\Pi_i$  satisfy Neumann conditions on-axis. Similarly, the variables corresponding to  $\omega_\alpha$  and  $\xi_\alpha$  that are evolved in the code have appropriate powers of  $\rho$  factored out so that they satisfy Dirichlet conditions on-axis (see [10] for the specific definitions).

For the evolutions presented here we use the following initial data for the scalar field components

$$\begin{aligned} \Phi_{r|i}(\rho, z, 0) &= A_{r|i} \exp \left[ - \left( \sqrt{\rho^2 + z^2} - R_{r|i} \right)^2 / \Sigma^2 \right], \\ \Pi_{r|i}(\rho, z, 0) &= \epsilon_{r|i} \Phi_{r|i}(\rho, z, 0), \end{aligned} \quad (11)$$

where  $A_r, A_i, R_r, R_i, \Sigma, \epsilon_r$  and  $\epsilon_i$  are parameters fixing the shape of the initial scalar field profiles. All other freely specifiable variables are set to zero at  $t = 0$ , while the constrained variables  $\alpha, \psi$  and  $\{\beta^\rho, \beta^z, w_\rho\}$  are obtained by solving the maximal slicing condition, Hamiltonian and momentum constraints respectively.

We use a partially constrained finite-difference scheme with adaptive mesh refinement (AMR) to evolve the system of equations with time. In particular, the slicing condition and momentum constraints are used to fix  $\alpha$  and  $\{\beta^\rho, \beta^z\}$  respectively, while the remainder of the variables are updated using their evolution equations.

## II. RESULTS

We now present results from a preliminary study of the black hole threshold of the complex scalar field system introduced in the previous section. We focus on four sets of initial data, summarized in Table I. Family **A** is the ‘canonical’ example, consisting of identical pulses of  $\Phi_r(\rho, z, 0)$  and  $\Phi_i(\rho, z, 0)$  that are initially approximately outgoing ( $\epsilon_r = 1$ ) and ingoing ( $\epsilon_i = -1$ ) respectively. This choice for  $(\epsilon_r, \epsilon_i)$  in a sense maximizes the net angular momentum (5), given the initial profiles for  $\Phi_r$  and  $\Phi_i$ . Conversely, family **B** is time-symmetric, and hence has zero net angular momentum. Families **A** and **B** can be written as  $\Phi(\rho, z, 0) = A(\rho, z) e^{i\delta_0}$ , where  $A(\rho, z)$  is a real amplitude function and  $\delta_0$  is a *constant* phase factor, equal to  $\pi/4$  in both cases. Family **C** is thus identical to family **A** except for the initial phase. For family **D**  $\Phi_r$  and  $\Phi_i$  have distinct initial profiles and thus cannot be characterized by a constant phase.

Based upon the collapse simulations we have performed for these four families of initial data, we can suggest the following about the threshold behavior for

Label	$p$	$R_r$	$R_i$	$\Sigma$	$\epsilon_r$	$\epsilon_i$	$\delta_0$	$\delta^*$
<b>A</b>	$A_r = A_i$	0.6	0.6	0.1	1	-1	$\pi/4$	$0.91 \pm 3\%$
<b>B</b>	$A_r = A_i$	0.6	0.6	0.1	0	0	$\pi/4$	$\pi/4$
<b>C</b>	$A_r = 3A_i$	0.6	0.6	0.1	1	-1	$\tan^{-1} \frac{1}{3}$	$0.39 \pm 3\%$
<b>D</b>	$A_r = A_i$	0.65	0.6	0.1	1	-1	—	$1.34 \pm 3\%$

TABLE I: Parameters (see (11)) for the four families of initial data discussed here, where  $p$  denotes the parameter(s) we tune when searching for the black hole threshold.  $\delta_0$  and  $\delta^*$  are the phase of the initial data (if applicable) and estimated phase of the critical solution respectively. All of the simulations were run with the outer boundary  $(\rho_{\max}, z_{\max}, -z_{\min})$  at 4 (except for the data of Fig. 4, where the outer boundary was at 16), and in each case  $p$  was tuned to within  $(p - p^*)/p^* \approx 10^{-14}$  of threshold.

this matter model. There *is* apparently a discretely self-similar critical solution that is universal to within a family-dependent phase. In other words, one can write the critical solution  $\Phi^*$  for the scalar field as  $\Phi^*(\rho, z, t) = A^*(\rho, z, t)e^{i\delta^*}$ , where  $A^*(\rho, z, t)$  is a universal real function and  $\delta^*$  is a family dependent constant (see Table I). Note that this phase dependence is a consequence of the  $U(1)$  symmetry of the Lagrangian of the complex field, and has been observed in charged scalar field critical collapse[11]. Also, note that *any* self-similar solution is unique only up to a global rescaling of the form  $(\bar{t}, \bar{x}^i) \rightarrow (\kappa\bar{t}, \kappa\bar{x}^i)$  when written in suitable coordinates  $(\bar{t}, \bar{x}^i)$ , with  $\kappa$  a constant. Fig. 1 shows a snapshot of the real part of the scalar field  $(\Phi_r \rho)$  at late times in a near-critical collapse simulation. To estimate  $\delta^*$  for a given family, and the echoing exponent  $\Delta$  for the putative critical solution, we examine the central value of the real and imaginary parts of the scalar field divided by proper radius  $\rho_c$  (to factor out the leading order approach to 0 of  $\Phi$  in a covariant manner)

$$\rho_c \equiv \rho \psi^2 e^{\rho \bar{\sigma}}. \quad (12)$$

Fig. 2 shows plots of  $\Phi_r \tau \rho / \rho_c$  and  $\Phi_i \tau \rho / \rho_c$  vs.  $-\ln \tau$  for the nearest-to-threshold solutions found, where  $\tau$  is central proper time (see [5] for our definitions and computations of quantities measured by central observers, but note that we define  $\tau$  such that the accumulation event of the critical solution corresponds to  $\tau = 0$ ). We have multiplied the scalar field by  $\tau$  in these plots to cancel the artificial growth introduced by dividing by  $\rho_c$ . Note that the equations of motion for  $\Phi_r$  and  $\Phi_i$  are identical; hence if  $\Phi_r(\rho, z, 0) = \Phi_i(\rho, z, 0)$  (as with family **B**), then the initial phase,  $\delta_0 = \pi/4$ , is preserved during evolution. The echoing exponent  $\Delta$  is the period of the self-similar solution in logarithmic proper time; from Fig. 2 (and similar data for family **B**) we estimate  $\Delta = 0.42 \pm 4\%$ . To estimate the scaling exponent  $\gamma$ , we measure how the maximum value attained by the Ricci scalar (on axis),  $R_m$ , in sub-critical evolutions depends upon the parameter-space distance from threshold,  $p^* - p$  [12]. Representative re-



FIG. 1: A surface plot of the real part  $(\Phi_r \rho)$  of the complex field after several echoes of a near-critical evolution. The origin is at the bottom-center of the figure, the  $\rho$  axis runs vertically through the middle, and the  $z$  axis runs horizontally. Only a single echo (roughly) at the origin corresponds to the self-similar part of the spacetime—the other “waves” visible were radiated during earlier echoes of the field. Note also that the solution is *not* spherically symmetric.

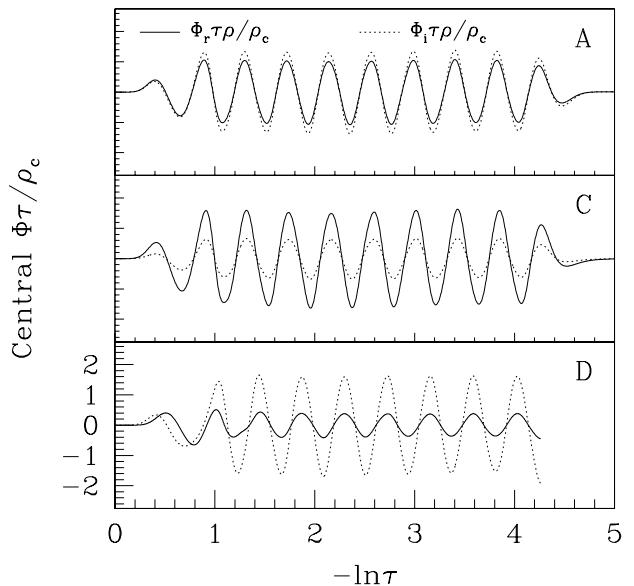


FIG. 2: The real  $(\rho\Phi_r)$  and imaginary  $(\rho\Phi_i)$  components of the central value of  $\Phi$  (9) multiplied by proper time  $\tau$  and divided by proper radius  $\rho_c$  (12), versus  $-\ln \tau$  for the near-critical collapse solutions of families **A**, **C** and **D** (the phase information for family **B** is trivial as  $\Phi_r = \Phi_i$  then, and so for brevity we do not show it). The family **D** solution shown here is super-critical, and the simulation is stopped soon after an apparent horizon is detected.

sults are shown in Fig. 3. Combining such data from all the families, we estimate  $\gamma = 0.11 \pm 10\%$ . For a discretely self-similar solution, one expects the linear relationship assumed in Fig. 3 to be modulated by an oscillation of period  $2\Delta$  [13]; we have not run a sufficient number of simulations to adequately resolve such an oscillation.

The uncertainties quoted above for  $\gamma$ ,  $\Delta$  and  $\delta^*$  (in Table I) were estimated from convergence calculations from simulations using 3 different values of the maximum truncation error threshold that controls the AMR algorithm, but do not account for possible systematic errors (see a

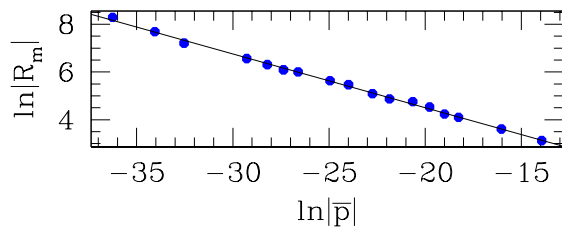


FIG. 3:  $R_m$ , the maximum value of the Ricci scalar on axis ( $\rho = 0$ ) attained during sub-critical evolution, versus distance  $|\bar{p}| = p^* - p$  from threshold, for family **A**. Each point represents a single simulation. The line is a least-squares fit to the data;  $R_m$  has dimension  $length^{-2}$ , and hence the slope of the fit is expected to be  $-2\gamma$ . For this case we infer  $\gamma \approx 0.11$ .

discussion of related issues in [5]).

Finally, as mentioned in the introduction, for the near-critical solutions described here, net angular momentum seems to be completely irrelevant. To within the accuracy of our simulations, we cannot differentiate between the late time, self-similar regions of the spacetimes obtained from families **A** or **B**, and in the latter case, there is *no* angular momentum. In fact, any angular momentum present is radiated away so rapidly during self-similar collapse that we cannot accurately calculate the corresponding scaling exponent (i.e. the remaining angular momentum is zero to within truncation error). Fig. 4 shows a plot of the mass estimate  $M_{AH}$  versus angular momentum  $J_{AH}$ , on a logarithmic scale, of black holes formed in super-critical collapse.  $M_{AH}$  and  $J_{AH}$  are calculated from the area and angular momentum of the apparent horizon respectively (using the dynamical horizon framework [14]), and are computed at the time the apparent horizon is *first* detected. For large black holes (i.e. those with  $M_{AH}$  of order the ADM mass), Fig. 4 suggests that  $J_{AH} \propto M_{AH}^2$ . However, this region of parameter space is “maximally” far from threshold, in that these are almost the largest black holes that we can form from initial data not already containing an apparent horizon. For somewhat smaller black holes, Fig. 4 shows a transition to a

relationship closer to  $J_{AH} \propto M_{AH}^6$ ; however, we are still far from threshold there, and furthermore are entering the regime where the angular momentum calculation is dominated by numerical errors. Thus, perhaps the only quantitative statement we can make regarding angular momentum scaling for this system is that  $J$  scales to zero significantly faster than  $J \propto M^2$ .

### Acknowledgments

The authors gratefully acknowledge research support from CIAR, NSERC, NSF PHY-9900644, NSF PHY-0099568, NSF PHY-0139782, NSF PHY-0139980, Southampton College and Caltech’s Richard Chase Tolman Fund. Part of this work was completed at the KITP, supported by NSF PHY99-07949. Simulations were performed on UBC’s **vn** cluster, (supported by CFI and BCKDF), and the **MACI** cluster at the University of Calgary (supported by CFI and ASRA).

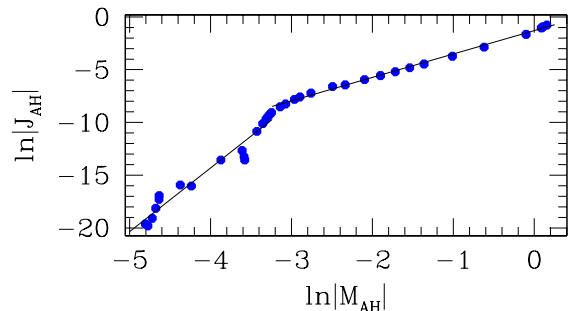


FIG. 4: Estimated black hole mass ( $M_{AH}$ ) versus angular momentum ( $J_{AH}$ ) in super-critical collapse of family **A** initial data. Points represent individual simulations, while the two lines are separate linear regression fits to the set of points to the left and right of the “knee” in the curve at  $\ln(M_{AH}) \approx -3.2$ , with slopes  $\approx 6.0$  and  $\approx 2.2$  respectively. In  $\ln \bar{p}$ , the horizontal scale ranges from  $-22$  to  $-2$  (compare to Fig. 3).

- 
- [1] M.W. Choptuik, *Phys. Rev. Lett.* **70**, 9 (1993)
  - [2] C. Gundlach, *Phys. Rept.*, **376**, 339 (2003); C. Gundlach, *Living Rev. Rel.* **2** 1999-4; A. Wang, *Braz.J.Phys.* **31**, 188 (2001)
  - [3] D. Garfinkle, C. Gundlach, and J. M. Martín-García *Phys.Rev.* **D59**, 104012 (1999)
  - [4] J. M. Martín-García and C. Gundlach, *Phys.Rev.* **D59**, 064031 (1999)
  - [5] M.W. Choptuik, E.W. Hirschmann, S.L. Liebling and F. Pretorius, *Phys.Rev.*, **D 68** 044007, (2003).
  - [6] M.W. Choptuik, I. Olabarrieta, W.G. Unruh and J.F. Ventrella, *in preparation*
  - [7] E.W. Hirschmann and D.M. Eardley, *Phys.Rev.* **D51** 4198, (1995)
  - [8] M.W. Choptuik, E.W. Hirschmann, S.L. Liebling and F. Pretorius, *Class.Quant.Grav* **20**, 1857 (2003)
  - [9] F. Pretorius, “Adaptive Mesh Refinement for Coupled Elliptic-Hyperbolic Systems”, in preparation.
  - [10] M.W. Choptuik, E.W. Hirschmann, S.L. Liebling and F. Pretorius, in preparation
  - [11] C. Gundlach and J.M. Martin-Garcia, *Phys.Rev.* **D 54**, 7353 (1996); S. Hod and T. Piran, *Phys.Rev.* **D 55**, 3485 (1996)
  - [12] D. Garfinkle and G.C. Duncan, *Phys.Rev.* **D58**, 064024 (1998)
  - [13] C. Gundlach, *Phys.Rev.* **D55**, 695 (1997); S. Hod and T. Piran, *Phys. Rev.* **D 55**, 440 (1997)
  - [14] A. Ashtekar and B. Krishnan, *Phys.Rev.Lett.* **89** 261101, (2002).